WELDING RESEARCH

SUPPLEMENT TO THE *WELDING JOURNAL*, JANUARY 2004
Sponsored by the American Welding Society and the Welding Research Council

Grain Boundary Character in Alloy 690 and Ductility-Dip Cracking Susceptibility

Grain boundary character and special boundary connectivity influence material resistance to ductility-dip cracking

BY V. R. DAVÉ, M. J. COLA, M. KUMAR, A. J. SCHWARTZ, AND G. N. A. HUSSEN

ABSTRACT. A complete elucidation of the physical mechanisms responsible for intermediate temperature ductility loss in metals (ductility dip) is elusive. This article provides insight pertaining to ductility-dip cracking in Alloy 690, namely that the fraction and interconnectivity of low-energy coincidence site lattice grain boundaries have a pronounced effect on material susceptibility to ductility-dip cracking. In this work, as-received wrought Alloy 690 is compared to Alloy 690 that was strain annealed to achieve a different configuration of special boundaries. Hot ductility tests are performed using a Gleeble™ thermomechanical simulator. It is shown that the intermediate temperature ductility dip is less pronounced in the strain-annealed material, that it is shifted toward lower temperatures, and that the on-cooling ductility recovery temperature (DRT) is higher. Scanning electron microscope fractographic analysis is coupled with electron backscattered diffraction (EBSD) pattern analysis to provide a preliminary metallurgical explanation of this improvement. It is qualitatively shown that improving the topological connectivity of these special boundaries in Alloy 690 enhances material resistance to cracking. Although this current study does not examine all possible factors contributing to ductility-dip cracking (DDC), it does suggest that grain boundary character and specifically the topological connectivity of special boundaries are important but, previously, not widely appreciated microstructural influencing factors in DDC.

V. R. DAVÉ and M. J. COLA are with the Nuclear Materials and Technology Division, Los Alamos National Laboratory, Los Alamos, N.Mex. M. KUMAR and A. J. SCHWARTZ are with the Chemistry and Materials Directorate, Lawrence Livermore National Laboratory, Livermore, Calif. G. N. A. HUSSEN is with the Materials Science and Engineering Department, Stanford University, Palo Alto, Calif.

Introduction

Alloy 690 is the material of choice for pressurized-water nuclear reactor components due to its superior stress corrosion cracking resistance as compared to Alloy 600. However, under heavy-restraint conditions, ductility-dip cracking during cooling from welding can be of concern (Refs. 1–3). The mechanism for DDC is unclear, and tests to determine susceptibility to DDC are often inconclusive. Ductility-dip cracking is uncharacteristic of other weld cracking mechanisms because it often occurs in alloys with low impurity levels. By contrast, heat-affected zone liquation cracking is directly related to boundary liquation resulting from elemental segregation at the grain boundaries or by liquated particles getting "swept up" by migrating boundaries. If the study of ductility-dip cracking is to be complete, consideration must be given to intrinsic components of the material, namely alloy chemistry and microstructure. In a previous investigation (Ref. 2), no evidence was found supporting the role of elemental segregation in the formation of ductility-dip cracks in Alloy 690. In this study, the role of the microstructural parameter of grain boundary character is addressed. The weldability issues addressed in this work focus on the relationship between the grain boundary character distribution, specifically the fraction and spatial distribution of certain types of grain boundaries, and how weldability may be improved by altering the grain boundary character.

KEY WORDS

Weldability
Alloy 690
Ductility-Dip Cracking
Grain Boundary Character Distribution
Special Grain Boundaries
Hot Ductility Testing

A complete background on the subject of grain boundary character is beyond the scope of this current work, but a brief introduction to the subject emphasizing recent developments is presented. Watanabe (Ref. 4) was one of the first researchers to realize that grain boundary character has a pronounced effect on material strength and ductility. Within the context of this work, grain boundary character is defined as the fraction and connectivity of so-called special or low-Σ boundaries. These boundaries are defined within the context of the coincidence site lattice (CSL) model for grain boundaries. Two adjacent grains are said to have coincident sites if for certain axes and angles of misorientation there are lattice sites in common. Kronberg and Wilson (Ref. 5) were among the first to utilize this concept to categorize the relationship between orientations before and after secondary recrystallization (high-temperature recrystallization) in copper. They found that the orientations could be related to one another by considering simple rotations about specific crystallographic axes. They postulated the concept of a coincidence plot that shows fraction of lattice sites in the new orientation that are coincident with sites in the old orientation. As Brandon (Ref. 6) points out, coincident grain boundaries, therefore, are those boundaries separating grains that have these special axes and angles of misorientation. The reciprocal density of coincident sites along certain close-packed planes is represented by the symbol Σ. Furthermore, in a cubic system, coincidence relationships exist for all odd values of Σ. Based upon empirical evidence, it is generally assumed that boundaries with $\Sigma \leq 29$ are low-Σ boundaries, i.e., those having many coincident sites, whereas those with $\Sigma > 29$ are called random boundaries (Ref. 7). Low-Σ boundaries, therefore, refer specifically to boundaries that are classified according

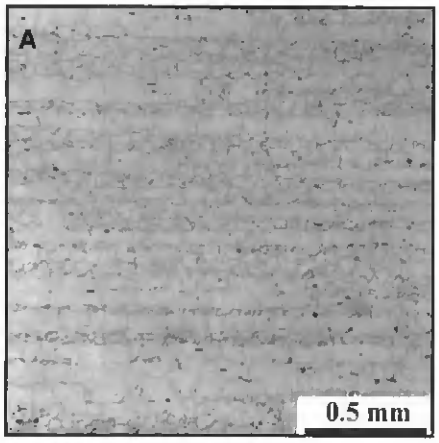

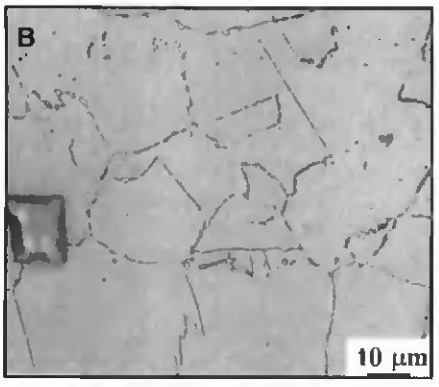

Fig. 1 — Alloy 690 as-received structure. A — Macrograph; B — micrograph showing carbides.

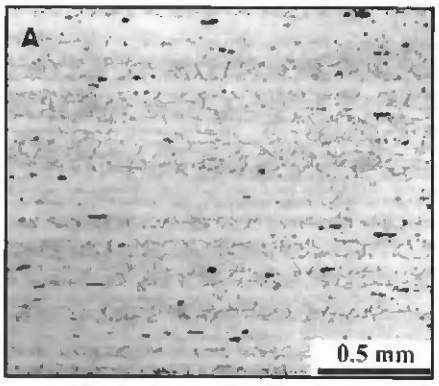

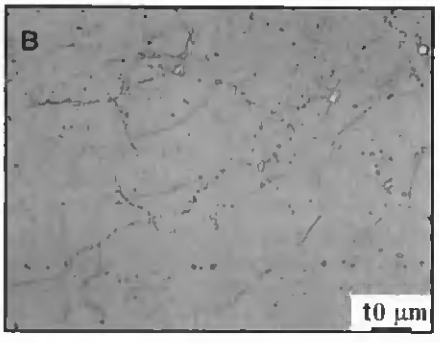

Fig. 2 — Structure of strain annealed Alloy 690. A — Macrograph; B — micrograph.

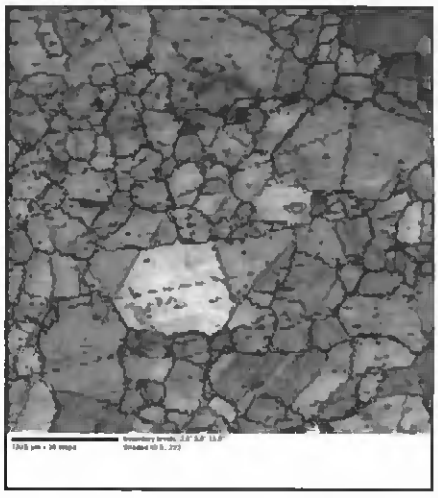

Fig. 3 — Orientation map of initial microstructure of Alloy 690.

to the CSL model. They are related to, but not entirely equivalent to, low-energy boundaries. For example, low-Σ boundaries are lower energy boundaries as compared to higher energy random boundaries, but simply classifying a boundary as being lower energy does not refer to a specific type of CSL boundary (a specific value of Σ). Grain boundary character distribution (GBCD) refers to the number of each type of boundary found in a microstructure and is commonly represented by a histogram in which the bins are ranges of values of Σ. Additionally and of equal importance is the concept that GBCD also implicitly relates to the spatial configuration of these boundaries, i.e., nature of the boundary network and various types of boundary junctions. Although there is no generally accepted way to represent the connectivity of low-Σ boundaries, this last point is of special significance in the present work and will be revisited at greater length later in this article. Recent experimental and theoretical work has suggested that the distribution of triple junction types classified according to how many low-Σ boundaries are coordinated is one simple measure of quantifying connectivity (Refs. 8–11).

The practical engineering significance of low-Σ boundaries is that they have special properties. Low-Σ boundaries are therefore also known as "special boundaries" since a preponderance of these boundaries are observed to confer enhanced properties such as damage and corrosion resistance. For example, Watanabe has shown that the presence of low-Σ boundaries results in a "structurally dependent" brittle-to-ductile transition (not to be confused with a temperature-dependent transition) occurring when the fraction of low-Σ boundaries increases beyond a certain threshold value (Refs. 12, 13). Additionally, it has been shown that a high fraction of special boundaries significantly enhances resistance to creep and grain boundary sliding at elevated temperature (Ref. 14). In materials that normally exhibit a very low strain-to-failure such as nickel aluminides, increasing the special boundary fraction significantly enhances the ductility and can increase strain-to-failure by up to a factor of four (Ref. 15). Also, in terms of intergranular corrosion and stress corrosion behavior, special boundaries in materials such as Alloy 600 have been observed to be virtually immune to intergranular corrosion effects (Ref. 16). Given such dramatic effects on a wide range of properties, it is therefore reasonable to assume that the grain boundary character distribution will have some influence on cracking behavior during welding, especially when this behavior is closely linked to intergranular failure, as is the case with ductility-dip cracking. Even for other weld cracking modes, such as heat-affected zone (HAZ) liquation cracking, there is some work that suggests that low-Σ boundaries are less susceptible to solute segregation and therefore more resistant to boundary liquation effects (Ref. 17).

Strain Annealing and Resulting Structure

Strain annealing and thermomechanical processing (TMP) in general is well established as a method for altering the grain boundary character distribution (Refs. 8, 18–20). There are, however, at least two different approaches in practice. The first approach relies on small strain increments on the order of 6–8% followed by annealing to cause grain boundaries to rotate toward lower energy configurations (e.g., Ref. 21). Alternatively, it is possible to impose moderate strain levels (~30%) followed by short high-temperature anneals (Refs. 8, 20). In this work, the as-received wrought mill product Alloy 690 is subjected to the following strain annealing sequence:

- Reduction in thickness 25% every cycle (four passes unidirectional rolling).
- Anneal at 1000°C for 1 h every cycle.
- Four cycles for a total reduction of about 67%.

Macro- and micrographs of the Alloy 690 structure before processing are shown in Fig. 1A and B. It is seen that the as-received structure has a banded mi-

crostructure and a bimodal grain size distribution (corresponding to the bands) resulting from thermomechanical processing. Figure 1B shows both types of carbides that are found in Alloy 690: the larger blocky MC (carbides of Nb, Ta, Ti, or V) are formed in the melt and are retained in the subsequent structure, whereas the finer $M_{23}C_6$ carbides decorating the grain boundaries form during processing. The corresponding macro- and micrographs for the material that underwent strain annealing are shown in Fig. 2A and B. Note that the banded bimodal grain distribution is maintained. Also, in Fig. 2B, strings of the $M_{23}C_6$ carbides away from the grain boundaries suggest that there has been some boundary migration and that these carbide strings mark former boundary locations.

Grain boundary character distribution is determined using orientation-imaging microscopy (OIM™, TSL Inc.) that utilizes the electron backscattered diffraction patterns to determine the orientation relationships between grains. The special boundaries ($\Sigma<29$) are color coded to differentiate them from the random boundaries that are shown in black. Figure 3 shows the orientation map for the initial material. The fraction of special boundaries is 40% in the as-received material. Previous work (Refs. 14, 18) suggests that significant shifts in properties occur when the special boundary fraction exceeds 60–70%. Figure 4A shows the OIM map after the strain annealing treatment. The special boundary fraction is elevated slightly to 50–55%. Perhaps of greater significance for this work is the connectivity of the random boundaries. This is shown in Fig. 4B for the Alloy 690 after strain annealing. What is noteworthy about this figure is that there are regions where the random boundary network has been significantly disrupted, and there are regions in which it is mostly intact. This is not surprising considering the banded nature of the initial as-received microstructure. Strain localization is expected in the regions with initially larger grains, and these regions therefore exhibited a greater breakup of the initial random boundary network. This variation in the connectivity of the random boundary network is of special significance in the discussion of the results. As will be shown below, the regions with the greater breakup of the random boundary network exhibit transgranular fracture, whereas regions in which the random boundary network is still intact fail in an intergranular manner.

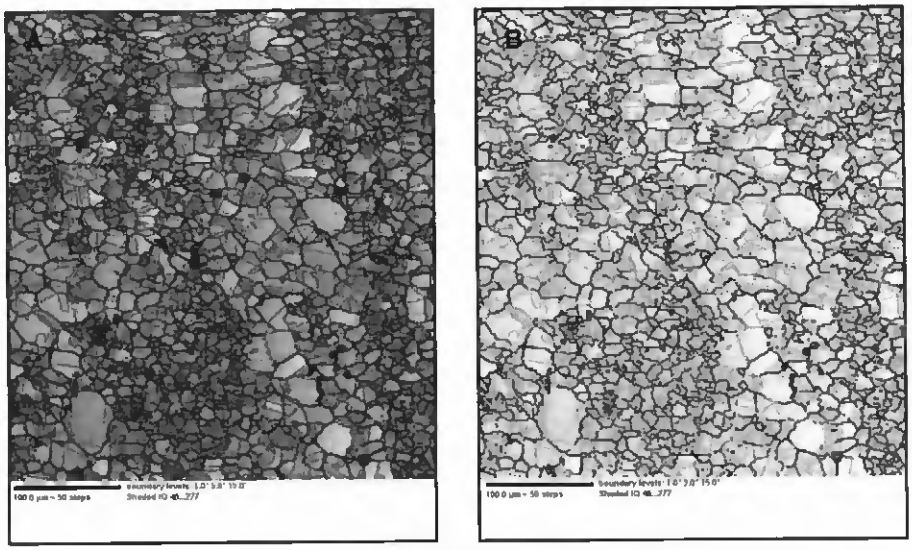

Fig. 4 — Orientation map of strain-annealed Alloy 690. A — Special boundaries in color; B — random boundaries in black.

Hot Ductility Testing and Fractographic Analysis

Material susceptibility to ductility-dip cracking is conveniently evaluated using Gleeble hot ductility testing. A model 1500 Gleeble thermomechanical simulator is used in this study. The on-heating rate is 111°C/s, and the on-cooling rate is 50°C/s. The on-heating tests are conducted as follows: heat at the specified on-heating rate until the target temperature is reached, strain until failure at 25 mm/s crosshead speed, and then measure the reduction in area on the specimens after removal from the test machine. The on-cooling tests are conducted as follows: heat at the on-heating rate until the nil-strength temperature (NTS is 1300°C for this ma-

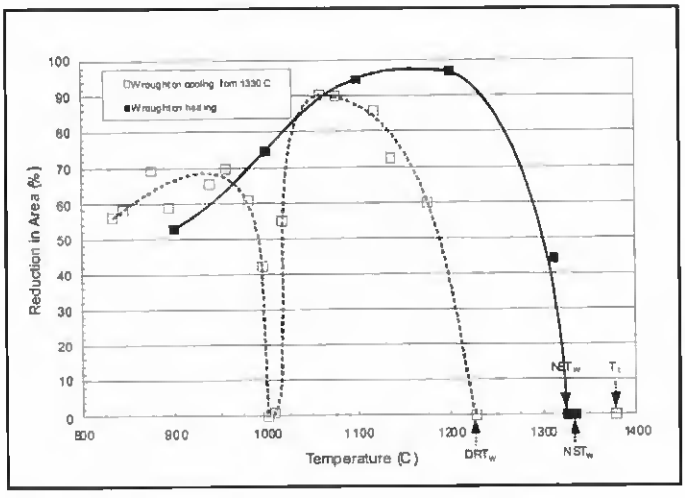

Fig. 5 — Hot ductility curves for as-received Alloy 690.

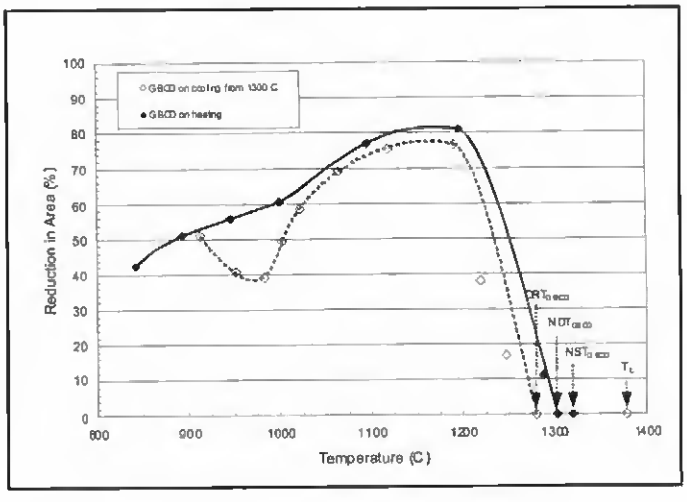

Fig. 6 — Hot ductility curves for strain-annealed Alloy 690.

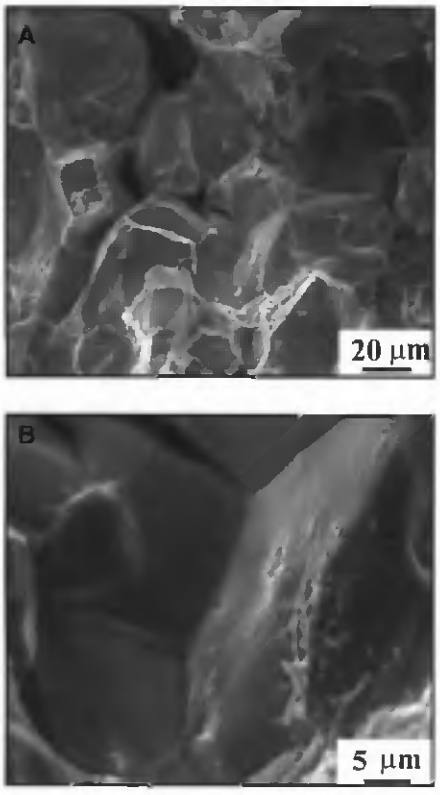

Fig. 7 — A — Fracture surface of as-received Alloy 690 tested on cooling at 1000°C; B — higher magnification.

terial) is reached, cool at the on-cooling rate, strain to failure at 25 mm/s stroke rate, and measure the reduction in area after the sample is removed from the machine.

The on-heating and on-cooling hot ductility data for the as-received Alloy 690 material are shown in Fig. 5. The on-cooling curve has a pronounced ductility dip at approximately 1000°C (950 to 1050°C) at which the reduction in area shrinks almost to zero. The strain does not in fact truly go to zero at this point, but it is certainly less than a few percent in terms of reduction in area. A calibrated shop caliper is used for all dimensional measurements in this study, but a more refined measurement could be made by digitally acquiring the image of the fracture surface and using image analysis software to calculate an effective reduction in area. However, based on several trials at the same conditions, the ductility dip for the as-received material is very severe, with a minimum value of less than 2% reduction in area. The implications of this dip on weldability are that a joint under extreme constraint could exhibit cracking on cooling from welding over the susceptible temperature range. For the strain-annealed material, the ductility curves are shown in Fig. 6. Of particular interest is the on-cooling curve, since it is most closely related to ductility-dip cracking in welding. The ductility recovery temperature is seen to be 50°C higher as compared to the as-received material; the ductility minimum is now 40% reduction in area as opposed to less than 2%; and the location of the minimum has shifted 25°C lower. It is reasonable to assume that this combination of a higher minimum ductility located at a lower temperature together with a higher DRT will result in increased material resistance to ductility-dip cracking on cooling from welding and thereby improve weldability for a given mechanical restraint condition.

A preliminary explanation for why the strain-annealed material exhibits a significantly different hot ductility response as compared to the as-received material can be postulated by combining the orientation maps with an analysis of the fracture surfaces. Figure 7A and B shows the fracture surfaces of a typical sample of the as-received material tested at the ductility minimum temperature of 1000°C on cooling. The fracture surface is intergranular with evidence of a slight "micro-dimpling" effect at very high magnifications on the otherwise smooth grain facet surfaces. Figure 8 shows the fracture surfaces of a typical strain-annealed sample tested at its corresponding ductility minimum temperature of 975°C on cooling. The fracture surface has a decidedly bimodal appearance. There are regions of intergranular fracture with lower reduction in area separated by regions of transgranular fracture that exhibited greater ductility. When these regions are compared to the previously shown grain boundary maps (Fig. 4A and B), it is seen that the regions in which the random boundary network was disrupted exhibited transgranular fracture, whereas the regions in which the random boundary network was largely intact exhibited intergranular fracture response.

Discussion and Conclusions

This work has resulted in several findings and observations that have direct implications on weldability in Alloy 690 and more specifically material resistance to ductility-dip cracking. First, it is shown that through strain annealing, it is possible to alter the grain boundary character distribution in Alloy 690. The processed material has slightly elevated fraction of special boundaries, but more significantly,

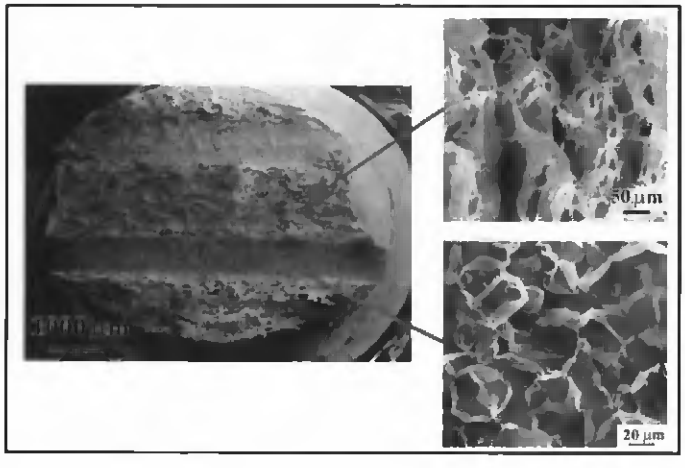

Fig. 8 — Bimodal appearance of strain-annealed Alloy 690 specimen tested on cooling at 975°C.

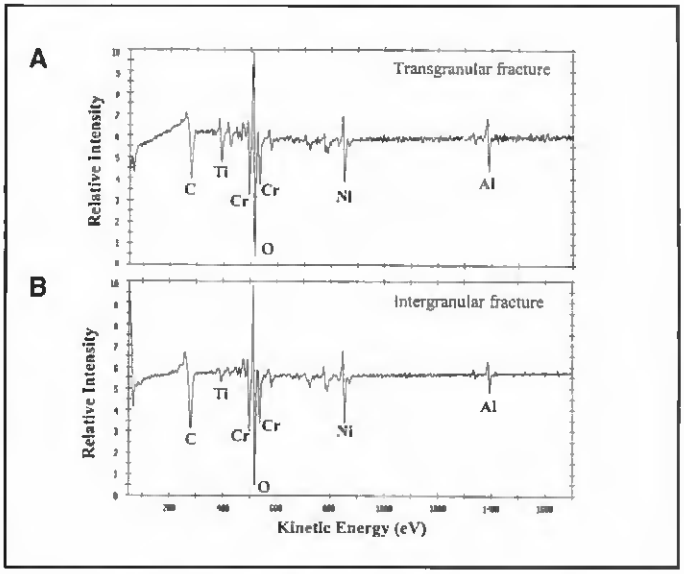

Fig. 9 — Auger spectra of regions exhibiting: A — transgranular; B — intergranular fracture.

there are regions in which the random boundary network was effectively disrupted. This is conversely equivalent to a greater connectivity of the special boundaries (as also discussed in Ref. 11). Furthermore, the processed material has a higher ductility recovery temperature, and a higher minimum ductility, and exhibits a shift in the position of the ductility minimum toward lower temperatures. All three of these factors are expected to favorably impact the material resistance to cracking and thereby improve weldability of Alloy 690 with respect to HAZ ductility-dip cracking. Lastly, a correlation exists between regions in which the random boundary network is disrupted and the tendency toward a transgranular fracture mode, thereby suggesting that grain boundary character and the topological interconnectivity of random boundaries are previously unappreciated microstructural influencing factors in ductility-dip cracking.

This work does not, however, unambiguously establish the linkage between a disrupted random boundary network and improved material resistance to DDC since there are several complicating factors. The first such factor is the banded nature of the initial microstructure. This bimodal structure is preserved during the strain annealing, thereby resulting in the complex fracture surfaces shown in Fig. 8. The material was chosen because it is a commercially used alloy and, as such, the aim of this study was to show relevance to actual engineering materials in use. Future work, however, should examine a material that does not exhibit such an initial structure. Then the effect of grain boundary character and connectivity of special boundaries can be more readily studied.

An additional complicating factor is the presence of carbides at grain boundaries and the fact that in some regions of the microstructure there was migration of the crystallographic boundaries leaving behind the $M_{23}C_6$ carbides. The effect of this migration on the ductility behavior was not fully elucidated in this work. Figure 9, however, does indicate that there is no evidence of liquation effects as determined by Auger analysis of the fracture surfaces. It is seen that the Auger spectra from transgranular and intergranular fracture surfaces are essentially identical, which would not be the case had there been any boundary liquation effect. Furthermore, the fracture morphology of the strain-annealed material in the regions exhibiting low ductility as seen in Fig. 8 does not resemble that which would result from liquation effects. Therefore, it is possible to rule out liquation as a factor with reasonable probability.

Other factors that could influence material resistance to DDC include grain boundary tortuosity and the orientation of boundaries with respect to the loading conditions imposed by joint restraint. The effect of these factors was not explicitly accounted for in this work. Therefore, the principal conclusion of this work is that a correlation between intact random boundary networks and intergranular brittle fracture modes was observed, and that, conversely, in regions where this random boundary network had been disrupted, transgranular ductile fracture occurred. This does suggest that grain boundary character and, more specifically, the topological connectivity of random (or conversely special) boundaries, do have an effect on material resistance to DDC, although there are other intervening microstructural factors. It is the authors' opinion that this has not previously been widely appreciated. Further studies on very pure materials (to eliminate any possible intervening effects of secondary-phase particles) that are subjected to various strain-annealing treatments may be able to further elucidate the effect of this structural variable on cracking behavior.

Acknowledgments

The authors from Los Alamos and Lawrence Livermore National Laboratories would like to acknowledge the support of the University of California, which administers both laboratories for the National Nuclear Security Administration of the U.S. Department of Energy. Note: this document has been approved for unlimited public release. V. R. Davé would also like to thank D. Scott Duvall, retired executive of Pratt & Whitney and AWS Fellow, for the initial encouragement for this work.

References

1. Lin, W., and Cola, M. J. 1997. Weldability of Inconel Filler Metal 52. *Abstracts of Papers, 1997 AWS Convention.* Los Angeles, Calif.

2. Cola, M. J., Teter, D. F., Papin, P. A., and Taylor, T. N. 1998. Optical and analytical electron microscopy of ductility-dip cracking in Ni-base Filler Metal 52 — Initial studies. *Fifth International Conference on Trends in Welding Research.* Callaway Gardens Resort, Pine Mountain, Ga.

3. Kikel, J. M., and Parker, D. M. 1998. Ductility dip cracking susceptibility of Filler Metal 52 and Alloy 690. *Fifth International Conference on Trends in Welding Research.* Callaway Gardens Resort, Pine Mountain, Ga.

4. Watanabe, T. 1984. Approach to grain boundary design for strong and ductile polycrystals. *Res Mechanica* 11(1): 47–84.

5. Kronberg, M. L., and Wilson, F. H. 1949. Secondary recrystallization in copper. *Transactions of AIME* 185(8): 501–514.

6. Brandon, D. G. 1966. The structure of high-angle grain boundaries. *Acta Metallurgica* 14(11): 1479–1484.

7. Watanabe, T. 1983. Grain boundary sliding and stress concentration during creep. *Metallurgical Transactions-A* 14(4): 531–54.

8. Kumar, M., King, W. E., and Schwartz, A. J. 2000. Modifications in the microstructural topology in FCC materials with thermomechanical processing. *Acta Materialia* 48:2081.

9. Minich, R. W., Schuh, C. A., and Kumar, M. 2002. Role of topological constraints on the statistical properties of grain boundary networks. *Physical Review B* 66:052101.

10. Schuh, C. A., Minich, R. W., and Kumar, M. 2002. Connectivity and percolation in grain boundary networks. *Philosophical Magazine A.* 83(6).

11. Schuh, C. A., Kumar, M., and King, W. E. 2002. Analysis of grain boundary networks and their evolution during grain boundary engineering. *Acta Materialia.*

12. Lim, L. C., and Watanabe, T. 1989. Grain boundary character distribution controlled toughness of polycrystals — A two-dimensional model. *Scripta Metallurgica* 23:489–495.

13. Lim, L. C., and Watanabe, T. 1990. Fracture toughness and brittle-ductile transition controlled by grain boundary character distribution (GBCD) in polycrystals. *Acta Metallurgica* 38:2507.

14. Lehockey, E. M., and Palumbo, G. 1997. On the creep behavior of grain boundary engineered nickel. *Materials Science and Engineering-A* A237:168–172.

15. Chiba, A., Hanada, S., Watanabe, T., Abe, T., and Obana, T. 1994. Relation between ductility and grain boundary character distributions in Ni_3Al. *Acta Metallurgica et Materialia* 42(5): 1733–1738.

16. Lehockey, E. M., Palumbo, G., Lin, P., and Brennenstuhl, A. M. 1997. On the relationship between grain boundary character distribution and intergranular corrosion. *Scripta Materialia* 36(10): 1211–1218.

17. Guo, H., Chaturvedi, M. C., Richards, N. L., and McMahon, G. S. 1999. Interdependence of character of grain boundaries, intergranular segregation of boron and grain boundary liquation in a simulated heat-affected zone in Inconel 718. *Scripta Materialia* 40(3): 383–388.

18. Palumbo, G. 1998. Metal alloys having improved resistance to intergranular stress corrosion cracking. U.S. Patent 5,817,193.

19. King, W. E., and Schwartz, A. J. 1998. Toward optimization of the grain boundary character distribution in OFE copper. *Scripta Materialia* 38(3): 449–455.

20. Kumar, M., Schwartz, A. J., and King, W. E. 1999. Modifications in the grain boundary character distribution in FCC materials through thermo-mechanical processing. *Proc. Inter. Conf. on Texture of Materials.* Montreal, Canada, August 9–13.

21. Thomson, C. B., and Randle, V. 1997. The effects of strain annealing on grain boundaries and secure triple junctions in Nickel 200. *Journal of Materials Science* 32(7): 1909–1914.